The Ernesto Cave, northern Italy, as a candidate auxiliary reference section for the definition of the Anthropocene Series

Andrea Borsato[1,2], Ian J. Fairchild[3], Silvia Frisia[1], Peter M. Wynn[4], Jens Fohlmeister[5]

[1] School of Environmental and Life Sciences, The University of Newcastle, Australia

[2] Museo delle Scienze, Trento, Italy

[3] School of Geography, Earth and Environmental Sciences, University of Birmingham, UK

[4] Lancaster Environment Centre, Lancaster University, UK

[5] Federal Office for Radiation Protection, Berlin, Germany

* Corresponding author: andrea.borsato@newcastle.edu.au

i.j.fairchild@bham.ac.uk

silvia.frisia@newcastle.edu.au

p.wynn@lancaster.ac.uk

jens.fohlmeister@gmail.com

Abstract:

Annually laminated stalagmites ER77 and ER78 from Grotta di Ernesto provide an accurate annual record of environmental and anthropogenic signals for the last ~200 years. Two major transitions are recorded in the stalagmites. The first coincides with the year 1840 CE, when a change from porous and impurity-rich-laminae to clean, translucent laminae occurs. This is accompanied by a steady increase in the growth rate, a decrease in fluorescence and a sharp increase in $\delta^{13}C$ values. These changes concur with the end of the Little Ice Age. The second transition takes place around the year 1960 CE and corresponds with an increase in both annual growth rate and sulphur concentration in stalagmite ER78 at 4.2 mm from the top, and with the deflection point in the ^{14}C activity curve in stalagmite ER77 at 4.8 mm from the top. This latter is the stratigraphic signal proposed as the primary guide for the definition of the Anthropocene Series . The following shift toward depleted $\delta^{34}S$–SO_4 in stalagmite ER78 suggests

that industrial pollution is a major source of sulphur. The interpretation of atmospheric signals (S, ^{34}S, ^{14}C) in the stalagmites is affected by attenuation and time lags and the environmental signals are influenced by soil and ecosystem processes, while other anthropogenic signals ($\delta^{15}N$, ^{239}Pu) are not recorded. For these reasons, the stalagmite record is here proposed as an auxiliary (reference) section rather than a global standard. In summary, Grotta di Ernesto contains one of the best stalagmite records documenting the Anthropocene, and one of only two stalagmite records where the S peak has been measured at high resolution.

Keywords:

Annual laminae, Anthropocene, calcite fabric, carbon isotopes, fluorescence, growth rate, radiocarbon, speleothems, sulphur, synchrotron XRF

Introduction

This special issue, part of the work of the Anthropocene Working Group (AWG), presents data on twelve candidate archives for definition of the Anthropocene Series. A primary record will be chosen for consideration as a Global boundary Stratotype Section and Point (GSSP). The other archives may serve as additional references (auxiliary sites) to assist in global correlation of the Anthropocene signals. At this stage, the Grotta di Ernesto site is put forward as an auxiliary site because of natural delays in recording some signals through the overlying soil and ecosystem and lack of detectability of some signals of radioactive fallout.

The preparatory activities of the Anthropocene Working Group, including events leading to the submission of GSSP proposals and the binding decision that the base of the Anthropocene should align with stratigraphic signals dating to the mid-20th century, are detailed in the introductory article to this special issue (Waters et al., 2022).

Speleothems, and in particular annually laminated stalagmites, are increasingly being utilized for high-resolution paleoenvironmental and paleoclimate reconstructions as the presence of growth laminae ensures an annually resolved chronology, and their thickness and chemical composition are valuable proxies of paleoclimate information (Baker et al., 2021).

In this regard, Grotta di Ernesto is an excellent site because it is largely undisturbed and contains numerous active annually laminated stalagmites (Frisia et al., 2003). Moreover, it is one of the most extensively monitored cave sites worldwide where detailed hydrochemical monitoring, which has been carried out since 1993, established the relationships between speleothem proxy data and climate and environmental parameters (Borsato, 1995, 1997; Borsato et al., 2007, 2015a, 2015b, 2016; Huang et al., 2001; Fairchild et al., 2000, 2001; Frisia and Borsato, 2010; Frisia et al., 2000, 2003, 2005, 2008, 2011; Johnston et al., 2013; McDermott et al., 1999; Miorandi et al., 2010; Scholz et al., 2012; Smith et al., 2006, 2009; Wynn et al., 2010, 2013, 2014, 2018).

Grotta di Ernesto came to light in the autumn of 1983, during excavation work for the construction of a forest road in the municipality of Grigno (Trento). In July 1984, the Museo Tridentino di Scienze Naturali (now Science Museum of Trento), began a systematic exploration and archaeological survey and started an excavation intervention coordinated by Dr. G. Dalmeri. The cave, in fact, provided data on Mesolithic (ca. 9000 years BP) hunter-gatherers subsistence strategies related to ibex and red deer hunting (Dalmeri, 1985). At the conclusion of the archaeological research, the Cultural Heritage Service of the Autonomous Province of Trento, promptly proceeded to safeguarding the cave by closing its entrance with a solid iron door, thus preventing human and animal intrusion as well as excessive air circulation. In the following years the cave became the subject of further in-depth paleoethnological and paleoenvironmental investigations (Awsiuk et al., 1994).

Monitoring of soil and cave air pCO_2, drip water chemistry and *in-situ* calcite precipitation allowed recognizing that calcite crystals mostly grow during the cold season, when cave CO_2 concentration is at its lowest. This enhances dripwater CO_2 degassing, hence raising the pH and the calcite supersaturation of the solution (Fairchild et al., 2000; Frisia et al., 2000, 2010; Huang et al., 2001; Miorandi et al., 2010).

The Holocene climate variability at Grotta di Ernesto was studied in detail by comparing the annual growth rate, fabrics, geochemical and isotopic composition of three stalagmites (ER76, ER77, ER78). All three stalagmites show visible laminae for most of their growth, which commenced ca. 8500 yr BP (McDermott et al., 1999, Scholz et al., 2012). Each lamina is a couplet consisting of a translucent, non-fluorescent calcite layer (up to ~200 μm thick) and a thin brown (0.5-4 μm) fluorescent calcite layer enriched in soil-derived organic matter and a number of trace elements (Borsato et al., 2007; Fairchild et al., 2001; Frisia et al., 2000). Laminae are developed in calcite with a predominantly compact, columnar fabric for the past ca. 500 yr, and in porous, microcrystalline and dendritic fabrics in the mid and early Holocene (Frisia et al., 2000; McDermott et al., 1999; Scholz et al., 2012).

The development of annual lamination in stalagmite ER78 was further investigated by using synchrotron-radiation-micro-X-ray fluorescence (SR-μXRF) and ion microprobe analyses to reveal chemical variability across the visible layers (Borsato et al., 2007, Figure 1). A series of elements display gaussian-shaped peaks centered around the thin brown fluorescent calcite layer, with peak concentration intensity ordered Y > Zn, Cu and Pb > P and Br. This hierarchy reflects the selectivity of transport of these elements, which are bound to organic colloids flushed from the soil zone during autumn infiltration (Hartland et al., 2012). Ion microprobe analyses indicate that H, Na and F also increase (Fairchild et al., 2001). Sr displays a trough around the thin brown autumn layer, implying that its incorporation may be limited by competition with other elements and/or controlled by the growth mechanisms and growth rate (Borsato et al., 2007).

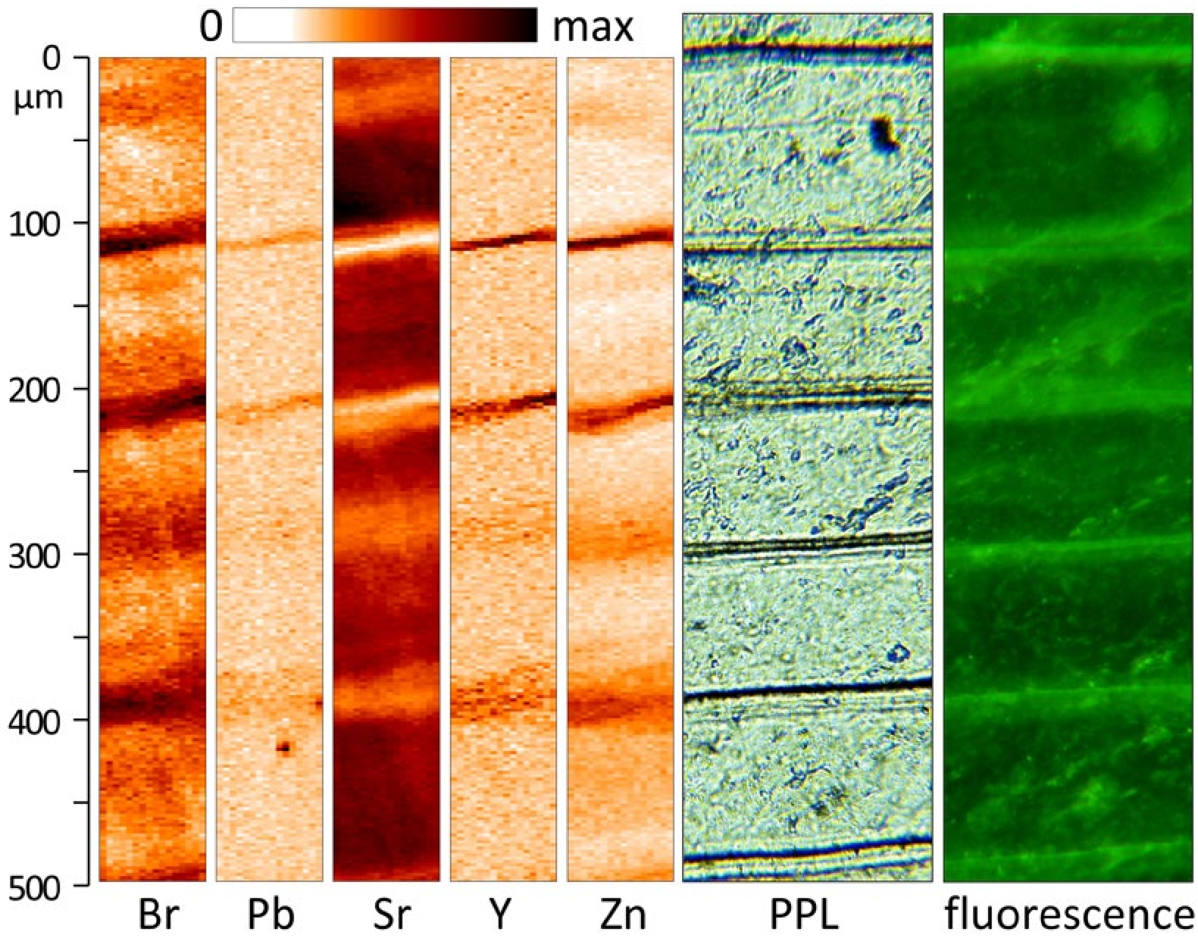

Figure 1. Annual laminae in stalagmite ER78 investigated with SR-µXRF (Borsato et al., 2007), optical (PPL plane polarized light) and fluorescence microscopy. Each lamina is a couplet consisting of a translucent, non-fluorescent calcite layer (~100 µm thick) enriched in Sr, and a thin brown fluorescent calcite layer enriched in soil-derived organic matter and a number of trace elements (Br, Cu, Pb, Y, Zn). In several laminae, the brown layer comprises a series of discrete thin (0.5-4 µm) layers, possibly marking distinct infiltration events.

Stalagmite growth rate at Grotta di Ernesto is positively correlated with surface air temperature (Frisia et al., 2003, Smith et al., 2006, 2009; Miorandi et al., 2010). By contrast, no such correlation exists with mean annual surface precipitation. Significant spectral density at 3, 7-8 and 11 years suggests an influence of both the North Atlantic Oscillation (NAO) and solar activity on stalagmite growth rates (Frisia et al., 2003). In particular, significant periodicities of ca. 7-8 and 3 yr, which are typical for the winter time NAO index, have been identified in ER76, ER77 and ER78 data series. Critically, the same periodicities were detected in instrumental temperature series of Northern Italy (Frisia et al., 2003). Spectral analysis of the $\delta^{13}C$ and $\delta^{18}O$ records of ER76 revealed that climate variability at Grotta di Ernesto was influenced by both solar activity and the NAO throughout the Holocene, which led to the identification of six periods of warm winter climate with a duration between 100 and 400 years centered at 7.9, 7.4, 6.5, 5.5, 4.9 and 3.7 ka (Scholz et al., 2012).

In the last two decades, cave monitoring also included the analysis of colloidal transport in dripwater (Hartland et al., 2012), as well as sulphate concentrations and sulphate isotopes in both drips and stalagmites, aimed at establishing a speleothem archive of atmospheric sulphur composition (Borsato et al., 2015b; Fairchild et al., 2009; Fairchild and Frisia, 2014; Frisia et al., 2005; 2008; Wynn et al., 2010, 2013, 2014). Soil carbon dynamics were investigated by analyzing the ^{14}C activity and $\delta^{13}C$ values of C dissolved in soil and cave drip water (Frisia et al., 2011). A 2-yr-long monitoring study also revealed a pronounced annual cycle in ^{14}C activity which is a function of drip-rate variability, soil moisture, and ultimately hydrology (Fohlmeister et al., 2010, 2011).

Materials and methods

Geographic and climatic setting

Grotta di Ernesto is located in the Province of Trento (Italy), in the Italian Pre-Alps (longitude 11°.65751 E, latitude 45°.97723 N) at 1167 m above sea level (asl). The cave opens on the north-facing slope of Sette Comuni karst plateau, and overlooks the Valsugana Valley (valley bottom at 230 m asl) (Figure 2). The cave consists of a single descending gallery, which opens into three successive chambers named (from the entrance to the innermost part) Sala del Focolare, Sala Grande and Sala Terminale, for a total length of ca. 70 m. Most of the passages are decorated by actively forming stalagmites, stalactites, flowstones, pools and spray deposits. The cave is cut in partially dolomitized, Jurassic limestone, overlaid by clay-rich calcareous brown soil (Calcari-Mollic Cambisols, pH 6.5–7.7) up to 100 cm thick. The present-day vegetation above the cave is a mixed conifer–deciduous forest association, composed of *Fagus sylvatica*, *Picea abies* and *Abies alba* (Fairchild et al., 2009; Miorandi et al., 2010). Most trees started to grow around 1920 CE, after the forest clearance carried out to facilitate military operations before World War 1 (Apolloni, 1996; Lageard et al., 2007). This major ecosystem disturbance is recorded in stalagmite ER78 by organic-rich laminae enriched in heavy metals (Cu, Pb, Y and Zn) in the period from 1900 to 1920 AD, which suggest enhanced leaching of trace elements through a disturbed soil profile (Borsato et al., 2007).

The north-facing cliff location of the cave results in cool temperatures at the surface, with mean monthly air temperatures ranging from 0° C during winter to 15°C during summer. Annual precipitation varied from 531 to 2268 mm/year between 1921 and 2007, with a mean value of 1289 mm/year. The majority of precipitation occurs in spring/early summer (May/June) and late autumn (October/November). Lagrangian computation of wind trajectories applied to a large ensemble of precipitation events in the region highlighted the important contribution of Mediterranean cyclones to local precipitation and a strong dispersion within 5-day back-trajectories (Bertò et al., 2004).

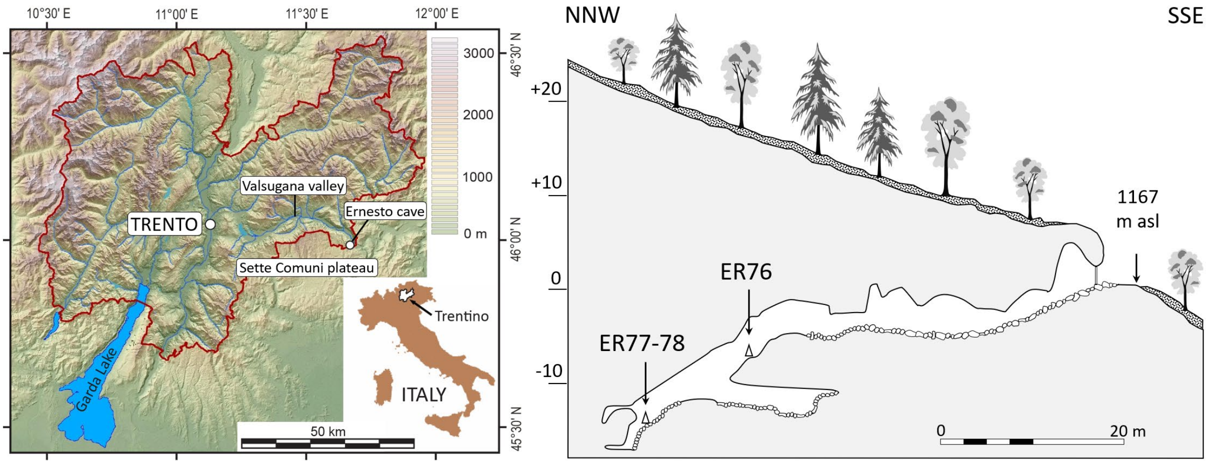

Figure 2. Location map and projected cross section of Grotta di Ernesto in Trentino (Province of Trento). The sampling sites of stalagmites ER76, ER77 and ER78 is shown.

Field collection of core, sampling and core imagery

For the study of Holocene climate and environmental variability, three active stalagmites were removed from the cave: ER76 (length 368 mm) in June 1993, ER77 (length 450 mm) in November 1995 and ER78 (length 60 mm) in October 2000 (Frisia et al., 2003). ER76 was taken towards the end of Sala Grande, whereas ER77 and ER78 were retrieved near the bottom of the cave (Figure 2). The entire stalagmites were extracted at their base by chisel and hammer and transported to the Science Museum in Trento. The stalagmites were then cut along their growth axis and the two halves were successively sliced in 10-12 mm slabs. The stalagmite slabs were then polished and scanned with a flatbed scanner (600 dpi resolution) (Figure 3) and used to obtain thin sections and carry out all geochemical analyses. Most of the stalagmite slices and thin sections are now archived in the geological specimen collection at the Science Museum in Trento. ER76, ER77 and ER78 are unique samples and it is not possible to obtain the same stalagmite material from the cave.

Uncoated 30 µm-thick, polished thin sections were obtained from the top section of stalagmites ER76, ER77 and ER78 and imaged by optical transmitted light with a Zeiss Axioplan microscope, and by fluorescent light stimulated by UV (365 nm) and blue wavelength (470 nm) lasers, with a Zeiss Axio Imager A1 fluorescence microscope.

Figure 3. Scanned images of ER76, ER77 and ER78 stalagmites cut along their growth axis. Note the characteristic translucent calcite layer in the topmost part of the three stalagmites (topmost 9 to 14 mm).

Chronological controls

ER76 stalagmite was dated by two series of U/Th analyses (McDermott et al., 1999; Scholz et al., 2012). The first batch was analysed using a Finnigan MAT 262 RPQ-2 mass spectrometer at University College Dublin, Ireland (McDermott et al., 1999) while the second series were analysed using a Finnigan MAT 262 RPQ thermal ionisation mass spectrometer (TIMS) with a double filament technique at the Heidelberg Academy of Sciences, Germany (Scholz et al., 2012). The age model of ER76 was then implemented by annual laminae counting (Frisia et al., 2003; Scholz et al., 2012). The annual layers were counted from the top down as far as the first hiatus at 19.8 mm dft (420 years) and between 42 mm dft and the base of the speleothem (368 mm dft) where no hiatuses were detected. This provided a floating, annually resolved chronology that was then adjusted to the U-series age model. The age for the base of the stalagmite was determined by minimising the average age difference between the U/Th and the lamina age models. The best agreement was obtained for a basal age of 8.038 ka, which is in good agreement with the U-series age model (i.e., 8.2±0.8 ka). Both age models generally show a good agreement, with the lamina counting age model always within the 95 % confidence limits of the U-series age model. This confirmed the annual origin of the lamination (Scholz et al., 2012). The topmost sections of stalagmites ER77 (24 mm) and ER78 (10 mm) were only dated by annual laminae counting, given that the annual origin of the laminae was confirmed by petrographic correlations, statistical and spectral analyses (Frisia et al., 2003; Scholz et al., 2012). The annual origin of the topmost section of stalagmite ER77 was further confirmed by radiocarbon analyses (Fohlmeister et al., 2011).

The layer counting was undertaken using thin section images obtained at the Zeiss Axioplan optical microscope. For stalagmites ER76 and ER78 the layer count was also carried out on fluorescent light images from thin sections stimulated by blue-wavelength (470 nm) lasers, obtained at the Zeiss Axio Imager A1 fluorescence microscope. The layer counting was performed along three separate alignments and by using discrete markers between different sections of the stalagmite (typically every 20–40 layers). The final distances and thicknesses were then calculated as the arithmetic averages of the three counts, and the counting error was evaluated from the discrepancy between the three counts.

Anthropocene proxies

The specimens for synchrotron-radiation-micro-X-ray fluorescence (SR-μXRF) analyses of ER78 stalagmite were prepared by double polishing a 200 μm-thick stalagmite slice cut in the axial portion, from which the thin section used to derive the age model was obtained (Frisia et al., 2003). The SR-μXRF experiments were performed at the ID21 and the ID22 beamlines of the European Synchrotron Radiation Facility. At the ID21 X-ray microscopy beamline, measurement of elements with low atomic numbers was performed (see Frisia et al., 2005 for analytical details). At the ID22 beamline, a 17.3 keV excitation energy allowed detecting the K-lines of all the elements up to Y and the L-lines of Pb, with an average detection limit of 0.06–0.15 ppm (depending on the element and the dwell time, Borsato et al., 2007).

Sulphur isotope analyses of speleothem carbonate were conducted on polished, gold-coated thin sections approximately 150 μm thick using a Cameca 1270 ion probe at the University of Edinburgh, School of Geosciences. $^{34}S/^{32}S$ ratios are expressed using the delta convention in per mil notation relative to VCDT (Wynn et al., 2010).

Samples for stable carbon and oxygen isotope ratios analyses were micromilled at 100 μm intervals in the upper 20 mm distance from top (dft) of ER77 and the upper 0 and 8 mm dft of ER76. The stable carbon and oxygen isotope ratios for the remainder of stalagmite ER76 were micromilled at ~250 μm intervals (Scholz et al., 2012). All measurements were performed using an on-line, automated carbonate preparation system linked to a triple collector gas source isotope ratio mass spectrometer at the University of Innsbruck. Values are reported relative to the VPDB standard. Precision of $\delta^{13}C$ and $\delta^{18}O$ values, estimated as 1σ standard deviation of replicate analyses, is 0.06 and 0.08 ‰, respectively.

Results

Petrography, microstratigraphy and chronology

ER76, ER77 and ER 78 consist entirely of low-Mg calcite (Frisia et al., 2000; Frisia and Borsato, 2010). A clear and sudden change from porous, opaque to compact translucent calcite (see fabric description in Frisia et al., 2000, 2003) is evident in their topmost section. The transition occurs at 9.8, 13.1 and 8.8 mm from the top in ER76, ER77 and ER78 respectively, coinciding with the year 1840±12 CE (Frisia et al., 2003).

The upper 150 laminae, which correspond to the interval from 1840 to 1991 CE, are typically ca. 100 µm thick and are stacked regularly to form a columnar fabric. Two bands of extremely reduced lamina thickness (4-20 µm) dominated by dark layers mark the period from ca. 1650 to 1713 and from 1798 to 1840 in ER76 and ER77 (in ER78 laminae are too thin to be resolved prior to 1840). These UV-luminescent, organic- and trace-element-enriched brown layers are clustered together to form 'dark bands' as observed with the optical microscope. Such bands typically occur in the 16^{th}-19^{th} centuries in all three stalagmites, and have not been observed in the mid-Holocene parts of ER76 and ER77. This suggests that the slowest growth rates occurred from ca. 1650 to 1840 CE, in the so-called 'Little Ice Age'. By contrast, some of the thickest laminae occur in the last 100 yr. This change reflects the consequences of surface air temperature increase following the end of the 'Little Ice Age' in the Italian Alps at around 1850 CE (Frisia et al., 2003, Smith et al., 2006).

In ER78, 165±25 laminae were counted in the topmost 9 mm, with a mean annual growth rate of 54.6±44 µm. At 2 mm dft, which coincides with the year 1984 CE, there is a sudden increase in growth rate up to 265±19 µm/year. This value stands up as exceptional in the whole series, as it surpasses by 4σ the mean annual growth rate of the uppermost 9 mm (Figure 4). The sudden and short-lived peak in the growth rate concurs with an increase in the Si content marked by a thin, micro-detrital layer. This marks the opening of the cave entrance in autumn 1983 followed by the archaeological excavation carried out during summer 1984 (Dalmeri, 1985). Another chronological marker in ER78 is a sharp peak in sulphur concentration at 8.4 mm dft (lamina age 1884±7 CE), which is likely to be related to the Krakatoa volcanic eruption in August 1883 (Frisia et al., 2005, 2008).

In stalagmite ER77 280±20 laminae were counted in the topmost 15.6 mm, with a mean annual growth rate of 55.6±50 µm. The passage between brown-fluorescent, porous microcrystalline to translucent, compact columnar calcite fabrics at 13.1 mm dft (lamina age 1841±10 CE) is marked by a steady increase in the growth rate (Figure 5).

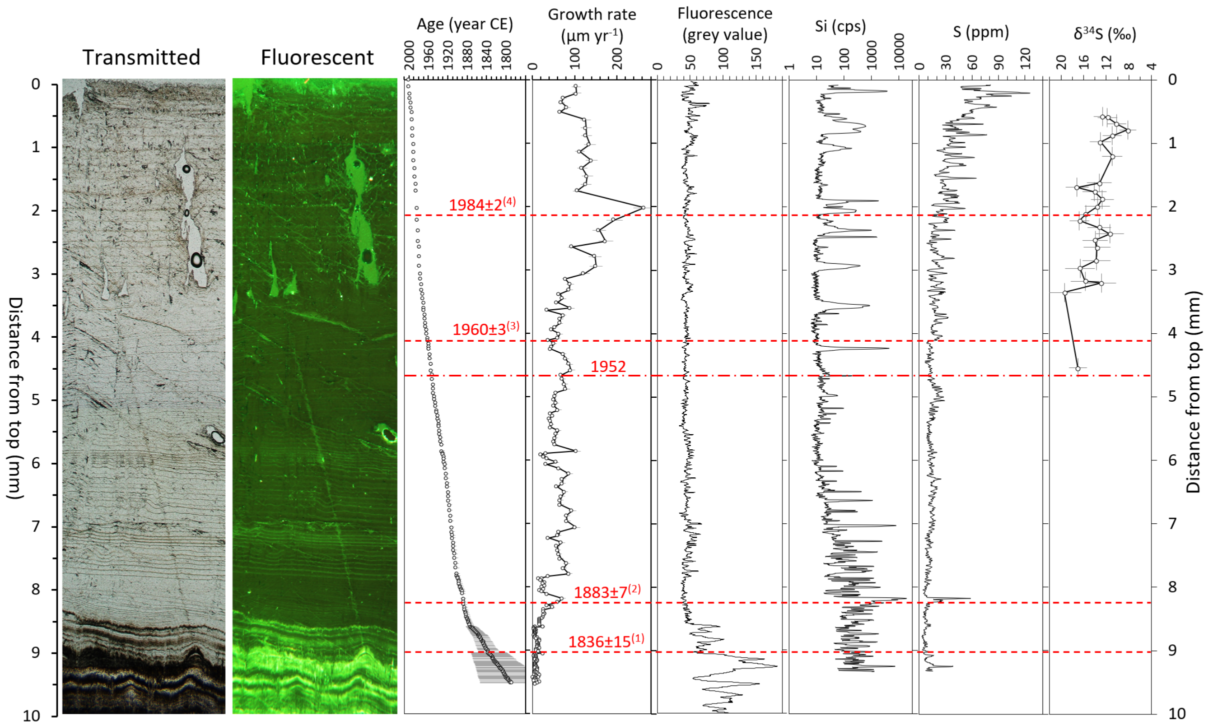

Figure 4. Thin section image in transmitted and fluorescent light (470 nm) of the topmost section of ER78 stalagmite compared with the annual growth rate and age model derived from layer counting (Frisia et al., 2003), the fluorescence signal (this work), the S and Si concentration composition (Frisia et al., 2005; Borsato et al., 2015), and $\delta^{34}S\text{-}SO_4$ (Wynn et al., 2010). Four time markers are highlighted: 1) The passage from porous microcrystalline to compact columnar calcite at 8.6 mm dft (lamina age 1836±16 CE); 2) the peak in sulphur concentration at 8.4 mm dft (lamina age 1884±7 CE), possibly related to the Krakatoa volcanic eruption in August 1883 (Frisia et al., 2005, 2008); 3) the increase in the annual growth rate and S concentration (lamina age 1960±3 CE), followed by the shift towards depleted $\delta^{34}S\text{–}SO_4$ that suggests an additional source of stalagmite sulphur originating from industrial pollution (Wynn et al., 2010); 4) the sudden increase of growth rate and Si content along a thin micro-detrital layer that corresponds to the opening of the cave entrance in autumn 1983 followed by archaeological excavations during summer 1984 (Dalmeri, 1985). Note the inverted scale for $\delta^{34}S$ and the logarithmic scale for Si (concentration reported in counts per seconds). The horizontal dash-dot line on 1952 is the reference to the first global Pu fallout, the preferred boundary for the Anthropocene Series (Water et al., 2018).

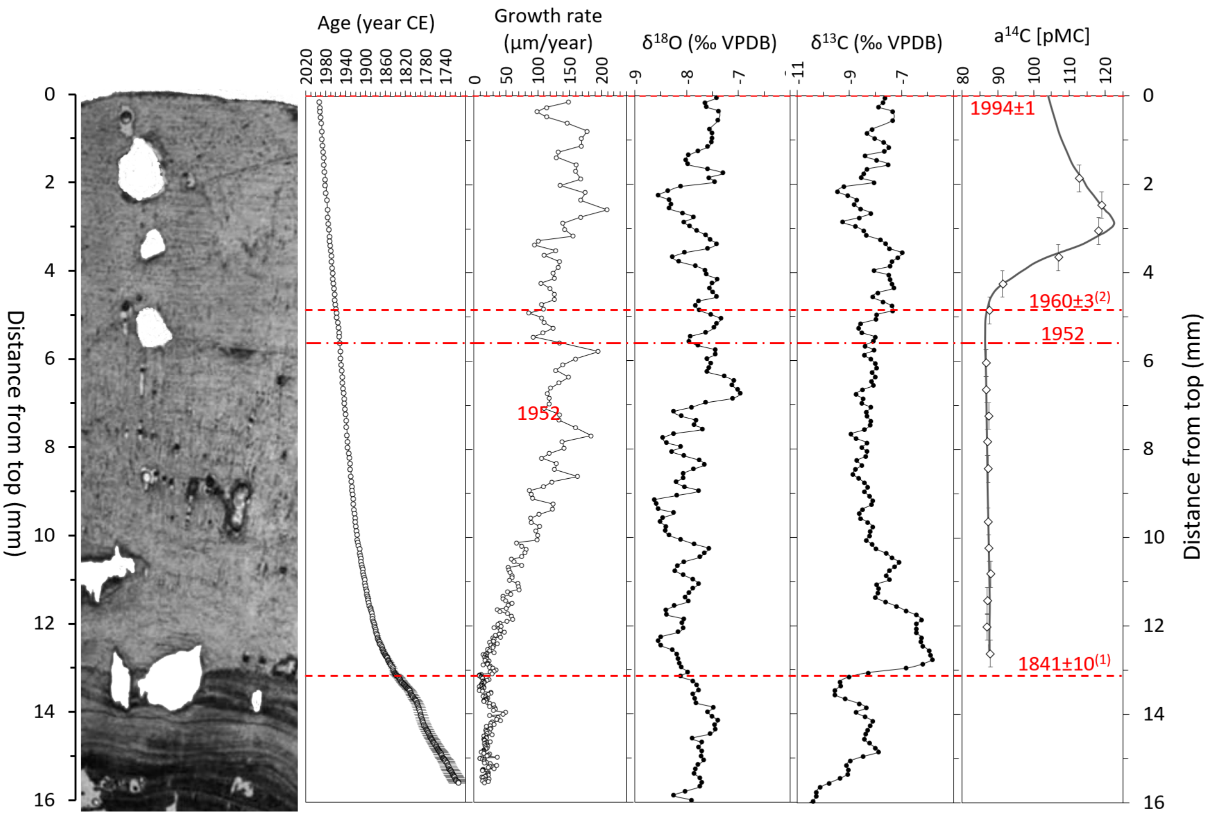

Figure 5. Thin section image in transmitted light of the topmost section of ER77 stalagmite compared with the age model derived from annual layer counting (Frisia et al., 2003), the oxygen and carbon isotope ratios (Scholz et al., 2012), and the ^{14}C activity (Fohlmeister et al., 2010). The grey line in the $a^{14}C$ graph is the modelled ^{14}C activity. Two time-markers are highlighted: 1) The passage from porous microcrystalline to compact columnar calcite at 13.1 mm dft (lamina age 1841±10 CE) marked by a steady increase in the growth rate and a sharp rise in $\delta^{13}C$; 2) the deflection point in the ^{14}C activity curve at 4.8 mm dft(lamina age 1960 CE) which corresponds to the stratigraphic signal proposed as the primary guide for the definition of the Anthropocene Series in stalagmite ER77. The horizontal dash-dot line on 1952 is the reference to the first global Pu fallout, the preferred boundary for the Anthropocene Series (Water et al., 2018).

Radioisotopes

Seventeen powder samples from the top 13 mm of stalagmite ER77 were obtained using a dental drill at a spatial resolution of 0.6 mm, resulting in a temporal resolution of 4 yr (in the 1970s) up to 10 yr (in the 1890s) depending on the growth rate. Due to technical limitations, it was not possible to drill the samples in a CO_2-free atmosphere. However, the background used (Iceland spar) did not show a significant enrichment in ^{14}C than other background samples, which were commonly drilled in a CO_2-free atmosphere. Therefore, the powdered samples were not affected by recent atmospheric $^{14}CO_2$ values (Fohlmeister et al., 2011). The calcite powders were acidified under vacuum and the evolved

CO_2 gas was dried and captured. This CO_2 was then combusted under a H_2 atmosphere to carbon, which was pressed into cathodes for accelerator mass spectrometry (AMS) analysis at the University of Lund AMS facility (Fohlmeister et al., 2011).

The Grotta di Ernesto ER77 stalagmite radiocarbon values can be precisely compared to atmospheric values because of the accurate age-depth control provided by the annual layer counting. The stalagmite ^{14}C measurements for the early 20th century reflect the atmospheric plateau-like behaviour (Figure 6). In addition, the slightly decreasing trend of ^{14}C atmospheric values in this period is well represented by the stalagmite data, although showing small fluctuations. The level of radiocarbon concentration (around 87 pMC) is on average about 13% less than that in the atmosphere and identifies the radiocarbon reservoir effect at the site. The ^{14}C reduction is attributed to dissolved carbon from the host-rock. However, a cave-site specific contribution to the reservoir effect can also originate from the ^{14}C age spectrum of soil organic matter (Noronha et al., 2015; Markowska et al., 2019). The best modelled fit with respect to the soil organic matter age spectrum of the measured data show a peak at 122.7 pMC in 1972.5 CE, with a delay of about 10 years with respect to the atmospheric ^{14}C activity peaking up to 197.3 pMC in 1963.6 CE (Figure 6). Therefore, the shape of the bomb peak in stalagmite ER77 is smoothed relative to the atmosphere and shifted towards younger times, which is likely related to the vegetation above the cave (Fohlmeister et al., 2011, Griffiths et al., 2012).A vegetation contribution to the radiocarbon reservoir effect is supported by the shape of the radiocarbon bomb peak in stalagmite ER77. The atmospheric radiocarbon levels in the mid to late 20th century underwent a rapid increase due to tropospheric nuclear weapon tests, resulting in an almost doubled radiocarbon concentration compared to the pre-bomb period. This was followed by a slower decrease in atmospheric ^{14}C back to almost pre-bomb peak levels.

Respired soil CO_2 at any given time contains C of the year (CO_2 from root respiration) and of older origin (microbial decomposition of old organic matter). For ER77 this resulted in a shift for the onset of the bomb peak by about five years. A 1- to 5-year delay of the deflection point is also often visible in other speleothems (Hua et al., 2017). The extent of the delay has been ascribed to processes related to transfer of the signal (via water) from soil to cave and to the ratio of soil CO_2 evolved from root respiration to that evolved from microbially decomposed old organic matter (Markowska et al., 2019). The peak of the bomb-pulse in stalagmite ER77 is shifted by about 10 years compared to the atmosphere. Furthermore, the peak ^{14}C values in the speleothem are about one fifth compared to the overall atmospheric radiocarbon increase. This can be explained by a smoothing action of the vegetation above the cave. Radiocarbon analysis of monthly collected drip water samples, performed in 2006 and 2007 CE, reveal mean values of ca. 101 pMC (Fohlmeister et al., 2011), which agree with the observed decline in the cave site-specific radiocarbon levels derived from the stalagmite measurements.

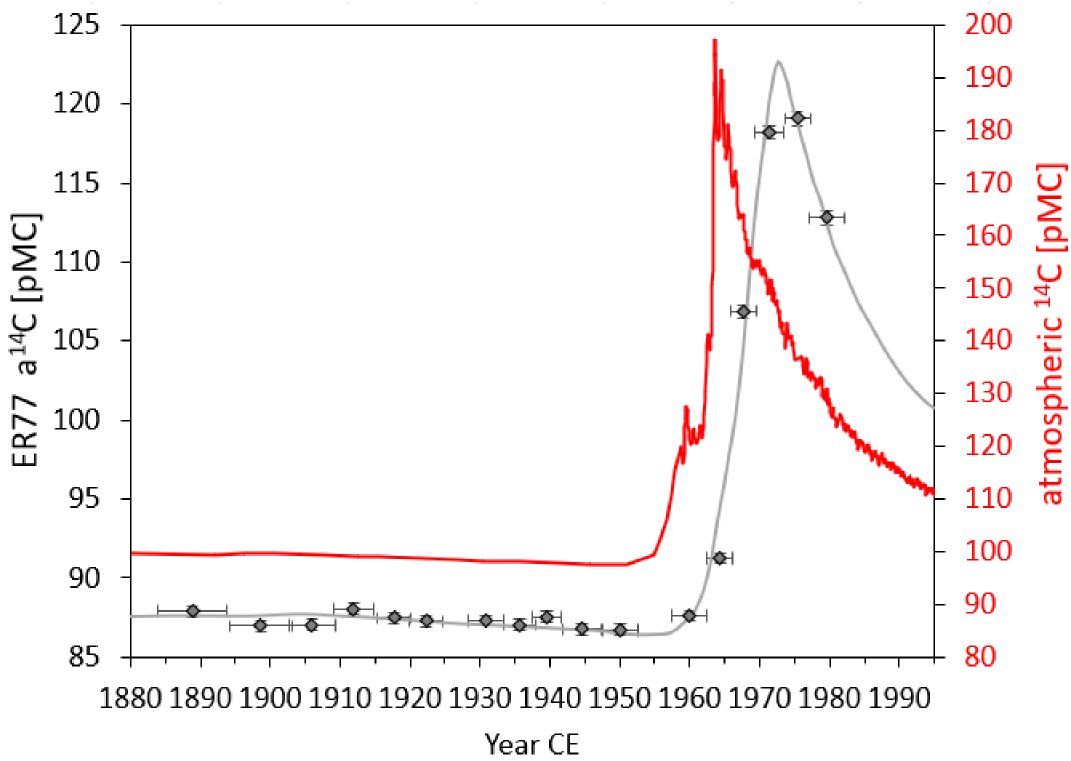

Figure 6. The atmospheric ^{14}C activity compared to ER77 stalagmite data (Fohlmeister et al., 2010). The atmospheric ^{14}C activity (red line) shows a plateau before 1950 CE, followed by the bomb pulse anomaly peaking up to 197.3 pMC in 1963.6 CE. The stalagmite data (black circles) are shown with 1-σ uncertainty in the ^{14}C measurements. The grey line is the best modelled fit with respect to the soil organic matter age spectrum of the measured data peaking at 122.7 pMC in 1972.5 CE. Note the different scales for the stalagmite and atmospheric pMC. The deflection point in the ^{14}C activity curve in year 1960 CE corresponds to the stratigraphic signal proposed as the primary guide for the definition of the Anthropocene Series in stalagmite ER77.

Geochemical and Organic Matter proxies

The comparison of the $\delta^{18}O$ records in ER76 and ER77 revealed that the $\delta^{18}O$ signal in Grotta di Ernesto stalagmites is influenced by several and partly competing factors (Scholz et al., 2012) that render its interpretation challenging. The influence of the amount effect to the $\delta^{18}O$ signal, as proposed in the first study (McDermott et al., 1999), was not confirmed by the $\delta^{18}O$ signal of the rainfall (Scholz et al., 2012), although reanalysis on the summer $\delta^{18}O$ signal in the region shows a positive, statistically significant linear correlation between rainfall $\delta^{18}O$ and rainfall amount (Johnston et al., 2021). The interpretation is further complicated by the fact that most of the summer precipitation, as well as a significant amount of snowfall in winter, does not contribute to the drip water balance of the stalagmites.

As a result, the $\delta^{18}O$ records in ER76 and ER77 do not show any particular trend, or clear feature, in the last 200 years (Scholz et al., 2012, Figure 5). On the other hand, spectral analysis of the stalagmite $\delta^{18}O$ signal revealed significant peaks at 110, 60–70, 40–50, 32–37 and around 25 years. With the exception of the 32–37 years cycle, all periodicities correspond to peaks in power spectra of NAO (25 years cycle) and solar variability (Scholz et al., 2012). This corroborates the spectral analysis of the lamina thickness of ER76, ER77 and ER78 stalagmites, which revealed high spectral density at 3 and 7-8 years (winter time NAO index) and 11 years (solar magnetic field cycles) (Frisia et al., 2003).

Monitoring data show that soil pCO_2, soil gas and water $\delta^{13}C$ values reflect temperature changes through the temperature sensitivity of vegetation cover, root respiration and bacterial decomposition of soil organic matter, with more negative $\delta^{13}C$ values corresponding to denser vegetation cover and warmer surface temperatures (Borsato et al., 2015a). However, drip water $\delta^{13}C$ values are also modified by dissolution of the host rock and rapid in-cave degassing of CO_2 as a response to cave ventilation (Frisia et al., 2011; Johnston et al., 2013). Grotta di Ernesto stalagmite $\delta^{13}C$ values, thus, reflect both vegetation and cave ventilation signals (Frisia et al., 2011; Scholz et al., 2012).

In stalagmite ER76, the millennial-scale decrease in $\delta^{13}C$ from 8.0 to 2.5 ka was interpreted as a progressive evolution in soil development and vegetation cover, in response to regional-scale warming (Scholz et al., 2012). On the other hand, the sharp shift from -10‰ to -6‰ at around 1841 CE in both ER76 and ER77, marked by a steady increase in the growth rate and a sudden shift from porous microcrystalline to compact columnar calcite (Figure 5), is related to the disturbance of the vegetation cover and enhanced cave ventilation. This event, marking the end of the Little Ice Age in this region of the Alps (Frisia et al., 2003), is likely a response to deforestation and associated disturbance in both soil and scree that obstructed the cave entrance. Deforestation above the cave caused the rapid degradation of the organic matter in the soil zone, whereas the disturbance in the scree enhanced cave ventilation and caused an increase in dripwater CO_2 degassing (Frisia et al., 2011). The disturbance of both vegetation and soil above the cave continued throughout the 19th century and, therefore, the stalagmite $\delta^{13}C$ signal likely reflects human activity and not specific climate events (Scholz et al., 2012).

Sulphur and sulphur isotopes

Sulphur concentration was first measured by S-µXRF analyses on ER78 stalagmite (Frisia et al., 2005, 2008) at the ESRF ID22 beamline in Grenoble. A 17.3 keV excitation energy made possible the detection of the K-lines of all the elements up to Y and of the L-lines of Pb, with an average detection limit of 0.06–0.15 ppm depending on the element and the dwell time (Borsato et al., 2007). Sulphur speciation as determined by XANES spectra (X-ray Absorption Near Edge Fine Structure), was dominated by sulphate species. S-µXRF relative concentration data were calibrated using absolute concentrations obtained from High Resolution Inductively Coupled Plasma Mass Spectrometry (HR-ICPMS) (Borsato et al., 2015b).

The sulphur concentration analyses revealed an increasing trend through time, which peaked in approximately 1997 (Frisia et al., 2005) and followed the trend in calculated sulphur emissions to the atmosphere associated with the anthropogenic combustion of fossil fuels (Mylona 1996, 1997; Vestreng et al., 2007; European Environmental Agency, 2014). The rising trend of sulphur concentrations from 1850 to the year 2000 (time of stalagmite removal from the cave) were then analysed by Secondary Ionisation Mass Spectrometry (SIMS) at the NERC ion probe facility of the University of Edinburgh, to identify the environmental source of sulphur.

Sulphur isotope data from 1850 to 1967 are omitted, due to low concentrations of sulphur (typically <20 ppm) causing poor precision of isotopic analysis (Wynn et al., 2010). Data from 1967 to 1995, demonstrate a secular shift in isotopic composition (Figure 7), with the isotopic signatures becoming depleted in ^{34}S towards the point of peak atmospheric emissions. Given that precipitation in the northern hemisphere sourced predominantly from anthropogenic emissions of SO_2 typically have a $\delta^{34}S$–SO_4 composition between −3 and +9‰ (Mayer, 1998), this shift was interpreted as representing increased atmospheric sulphur pollution relative to a background signal composed of sulphur sourced mainly from bedrock dissolution ($\delta^{34}S$–SO_4 bedrock signal ~20.5 ‰: Wynn et al., 2010).

Peak sulphur concentrations and isotopic signatures reflect the timing of peak sulphur emissions into the atmosphere prior to the introduction of environmental control measures, albeit displaying a time lag of approximately 20 years. This delay has been attributed to the uptake and biogeochemical cycling of sulphur through the vegetation, followed by transit through the karst. In this respect, it is interesting to note that the sharp S peak in 1889±6 CE, which was attributed to the 1883 CE Krakatoa volcanic event (Frisia et al., 2008), is delayed by only 6±6 years. This was interpreted as due to limited biogeochemical cycling related to cooling and less dense vegetation in the 19th century that favoured a faster transmission of the sulphur signal, with a delay similar to that of the mean residence time of the water within the aquifer (4–5 yr) (Borsato et al., 2015b).

The equivalent excursion in sulphur isotopic signatures can be seen within tree ring archives analysed from the vicinity of the cave (Wynn et al., 2014a). The isotopic fractionation associated with biogeochemical cycling is minimal under the oxidizing conditions typical of karst environments, and has little impact on the sulphur isotopic composition within the drip waters and speleothem archive in the cave below (Wynn et al., 2013). The onset of a return trajectory towards background sulphur signals relatively enriched in ^{34}S was not observed in ER78, due to the spatial resolution of analysis and the time of stalagmite collection, although it was recorded in the dripwater feeding the stalagmite a few years after stalagmite collection (Borsato et al., 2015b, Figure 7). By contrast, the return trajectory was observed in a speleothem from a nearby cave in the Austrian Alps, covering a slightly extended time-period of deposition (Wynn et al., 2010).

It appears that stalagmite ER78 identifies a true record of atmospheric sulphur emissions from anthropogenic combustion of fossil fuels. This can be reconstructed with a high degree of confidence imparted through the use of sulphur isotopes, albeit with a time delay of approximately 20 years between the point of emission to the atmosphere and appearance in the speleothem palaeorecord.

So far only another high-resolution S stalagmite record has been published from Obir cave in Austria (Wynn er at., 2014b). In this case, the delay is limited to approximately 10 years as the stalagmite peak occurs in the mid-1980s.

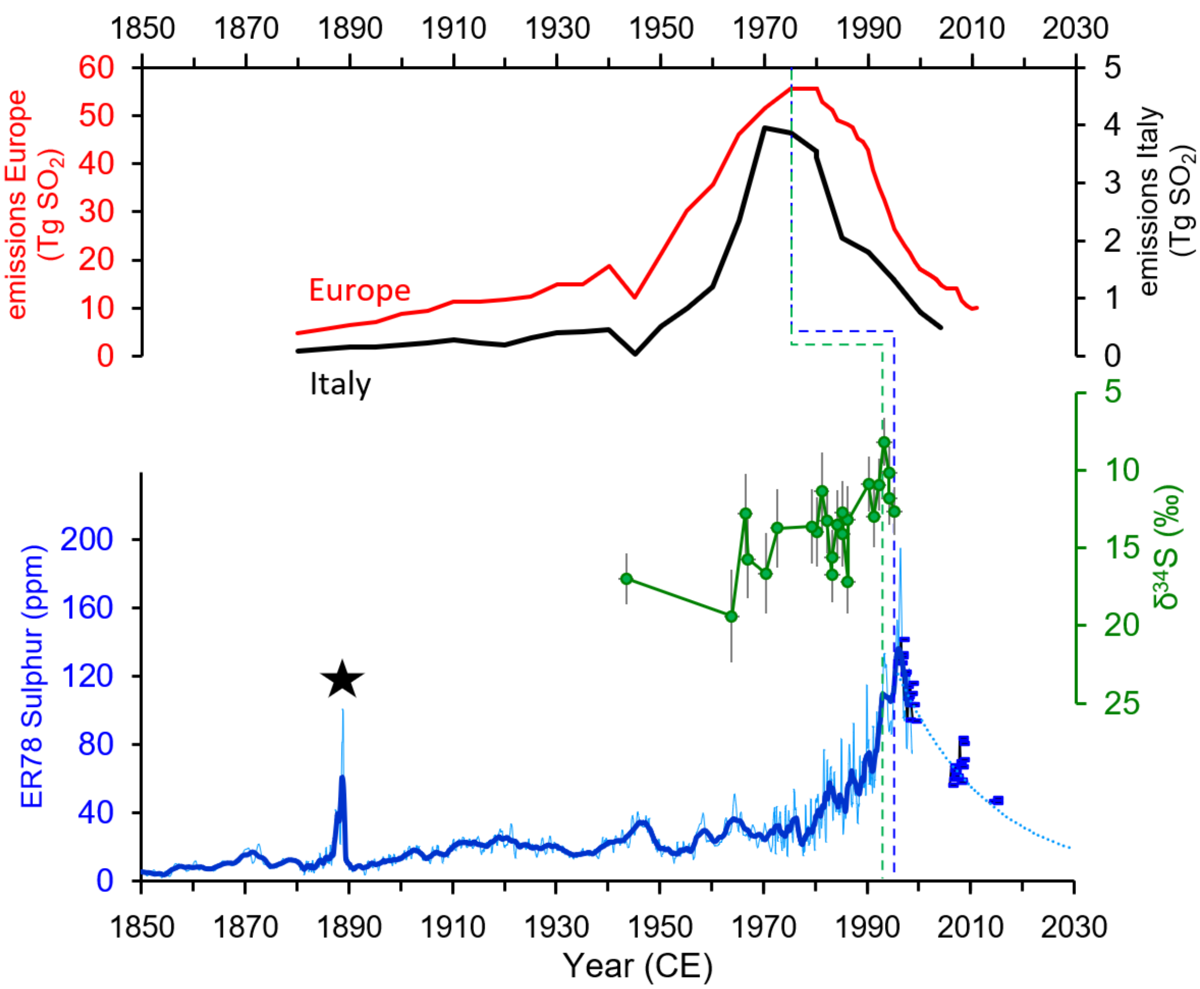

Figure 7. Sulphur and sulphur isotope records for ER78 stalagmite (Frisia et al., 2005; Borsato et al., 2015b; Wynn et al., 2010) compared with the sulphur dioxide emissions in Europe and Italy (Mylona 1996, 1997; Vestreng et al., 2007; European Environmental Agency, 2014). The sulphur actual data are shown by a blue thin line, whereas the bold line represents the 2-year Gaussian filter. The squared dots are the stalagmite series reconstructed by the measured dripwater S/Ca ratio for ER78 stalactite, and the dotted line the projected trend until 2030 (Borsato et al., 2015b). The green and blue dashed lines identify a delay of about 20 years between the peak in the sulphur dioxide emissions and the corresponding points in ER78 sulphur series due to biogeochemical cycling in the soil and vegetation above the cave (Wynn et al., 2013; Borsato et al., 2015b). The black star at 1889±6 CE marks the S peak, likely correlated to the Krakatau 1883 CE eruption (Frisia et al., 2008). Note the inverted scale for $\delta^{34}S$.

Discussion

Grotta di Ernesto is an excellent site for palaeoclimate and palaeoenvironmental studies being one of the most extensively monitored cave sites worldwide. Studies on the soil dynamics and transport of trace elements and organics through the aquifer facilitate the interpretation of the climate and environmental signals encoded in the stalagmites. The ubiquitous presence of visible annual laminae in the three studied samples implement the dating of the last few hundred years and makes the stalagmites the ideal material for precisely dated high-resolution studies.

A slow annual growth rate (around 100 μm/yr) and limited number of active stalagmites hindered the execution of additional analyses for which a large amount of material is required. The major problem in the evaluation of the anthropogenic signals encoded in the ER76, ER77 and ER78 stalagmites, however, is related to the modulation and smoothing action of the thick soil, the dynamic of cave ventilation and the vegetation cover, which has been strongly impacted by human activity in recent times. This is mostly evident in the trace-elements and in the $\delta^{13}C$ records. Trace metals linked to colloidal transport from the soil (Cu, Zn, Pb, Y) increased at the beginning of the 20th century as a result of deforestation (Borsato et al., 2007), whereas the $\delta^{13}C$ time series was strongly impacted by both deforestation and enhanced cave ventilation that took place around 1840 CE and shifted the $\delta^{13}C$ towards less negative values (Scholz et al., 2012). These processes completely masked the atmospheric Suess effect, the reduction of atmospheric $\delta^{13}C$ values by ~2‰ that has occurred since the start of the Industrial Revolution ~1820 CE. Such behavior is common in many recent speleothem records (Hua et al., 2017; Markowska et al., 2019) because stalagmite $\delta^{13}C$ values are dominated by the soil signal, given that soil CO_2 concentration is typically more than one order of magnitude higher with respect to the atmospheric values (Borsato et al., 2015b). The Suess effect, however, is noticeable in the radiocarbon pre-bomb period data. There is a slight, but robust decrease, mimicking the atmospheric one (Figure 6). This is plausible, as ^{14}C does not depend on soil dynamics and changes in cave ventilation as much as the $\delta^{13}C$ record (Frisia et al., 2011).

The modelled peak of the bomb-pulse in stalagmite ER77 occurred in 1972.5 CE, delayed by about 9 years compared to the atmosphere. The bomb pulse radiocarbon in the speleothem increases by about 30 pMC compared to pre-bomb times and, thus, is about one third compared to the overall atmospheric radiocarbon increase. The delay and reduction in the peak ^{14}C values are likely related to soil and vegetation above the cave and to the homogenising effect of the porous aquifer (Fohlmeister et al., 2011, Griffiths et al., 2012). The comparison with other stalagmite records worldwide clarifies the role of soil and aquifer in smoothing the atmospheric bomb-pulse ^{14}C signal. Two recent papers employed a new unsaturated zone C model which considers C decomposition as a continuum, to better understand ^{14}C dynamics (Markowska et al., 2019: Faraji et al, 2022 preprint). In particular, the study from two Cook Islands stalagmites from the South Pacific characterised by patchy soil cover and limited rock overburden that allowed a fast transmission of the atmospheric signal shows the highest peak pMC value (134.4) and the earliest inflection points (1956 and 1957 CE) documented worldwide in speleothems (Faraji et al., 2022 preprint). Remarkably, Pu17 stalagmite shows a sharp and early bomb peak in 1966, with a delay of just 2.5 years with respect to the atmospheric signal. On the other hand, stalagmites characterised by thick soil cover display much damped bomb ^{14}C rising and much lower peak pMC values (Markowska et al., 2019: Faraji et al, 2022 preprint). Overall, the ^{14}C record in ER77 is one of the most prominent and little-delayed records compared to over 20 stalagmite records published worldwide.

Whilst the stalagmite record represents an accurate reconstruction of environmental sulphur loading to the atmosphere, which can be traced to source using sulphur isotopes, the timing of the signal is modified by biogeochemical cycling and storage/mixing within the epikarst. The extent of signal modification is largely dependent on karst hydrology and antecedent soil dynamics. A karst system dominated by rapid fracture flow through soil and epikarst allows any modification by biogeochemical cycling to be bypassed. Likewise, if the ecosystem above the cave is replete in sulphur content, addition of sulphur in excess of that which can be taken up by the biomass will enter unmodified into the karst system beneath. However, in most environmental situations, biogeochemical cycling of sulphur in the soil-vegetation system above the cave will be extensive, leading to storage dynamics controlled by biomass recycling. In most instances, the redox conditions in the soil overlying karst bedrock will be predominantly oxidizing and the associated biogeochemical processes of assimilation (uptake of sulphur compounds into vegetation and soil biomass) and mineralisation (the return of carbon bonded sulphur compounds into the soil zone as sulphate) comprise only minimal net fractionation to the sulphur isotopes. Within the karst, storage and mixing with sulphate pools can further delay and modify the source sulphur signature. For stalagmite ER78, the archived sulphur signal originated predominantly from a pathway of biogeochemical cycling and storage/mixing in the karst. Isotopic integrity of the sulphur signal is retained, allowing tracing of sulphur signals to source, even though the timing of key events may be offset (Wynn et al., 2013).

When compared, the ER77 and ER78 stalagmite records show a similar behaviour (Figure 8), highlighted by two major events. 1) Year 1840 CE marked by the passage between microcrystalline impurity-rich to compact columnar laminae. This corresponds to the steady increase in the growth rate, the sudden decrease in fluorescence in ER78 and the sharp increase in $\delta^{13}C$ values in ER77 which mark the end of the Little Ice Age in this part of the Alps. It is important to note that the increase in the growth rate as well as the sharp increase in $\delta^{13}C$ values at around 1840 CE were also documented in ER76 stalagmite (Frisia et al., 2003; Scholz et al., 2012). 2) Year 1960 CE which corresponds to the proposed position of the GSSP in ER77 based on the deflection point in the ^{14}C activity curve, whereas in ER78 corresponds to the increase in the annual growth rate and S concentration, and the following shift towards depleted $\delta^{34}S–SO_4$ suggesting an additional source of sulphur originating from industrial pollution.

Ernesto Cave as a reference section for the Anthropocene Series

In summary, Ernesto Cave is so far one of the best cave sites documenting the Anthropocene, and is one of only two stalagmites where the S peak was measured at high resolution. Several anthropogenic indicators are clearly recorded in the three coeval stalagmites:

i) the growth rate increase as a consequence of the global temperature rise starting at around 1840 CE.
ii) the clear rise and peak in sulphur starting at around 1850 CE and peaking at 1997 CE.
iii) the enrichment in $\delta^{34}S$ starting at around 1960 CE and peaking at 1993 CE.
iv) the radiocarbon bomb-peak starting at around 1960 CE and peaking at 1972.5 CE.

An advantage of Ernesto Cave with respect to sedimentary sequences is that stalagmites are hard geological samples unaffected by possible diagenetic effects, and can be easily stored and displayed in museum collections and exhibits. Other actively growing stalagmites are present in the cave and they are potentially available for additional analyses and to cover the interval from year 2000 when the last of the three stalagmite (ER78) was collected. In fact, given the hydrological differences of stalagmites within the cave (Miorandi et al., 2010) it is likely that some of the Anthropogenic signals, in particular S concentration and ^{14}C can be replicated with lower attenuation and time lags.

On the other hand, several interferences and complications in the transmission of the atmospheric signal render the interpretation of the Anthropogenic proxies more difficult and argue against this site being the primary GSSP location. The concentration in heavy metals is linked to colloidal transport from soil, and their increase tends to reflect soil disturbance and/or deforestation events, masking the possible contribution of heavy metals (Pb) from atmospheric sources. At the same time, other atmospheric signals (S, ^{34}S, ^{14}C) have a tendency for attenuation and time lags, while some key Anthropogenic signals ($\delta^{15}N$, ^{239}Pu) (Waters et al., 2018) are absent or poorly presented.

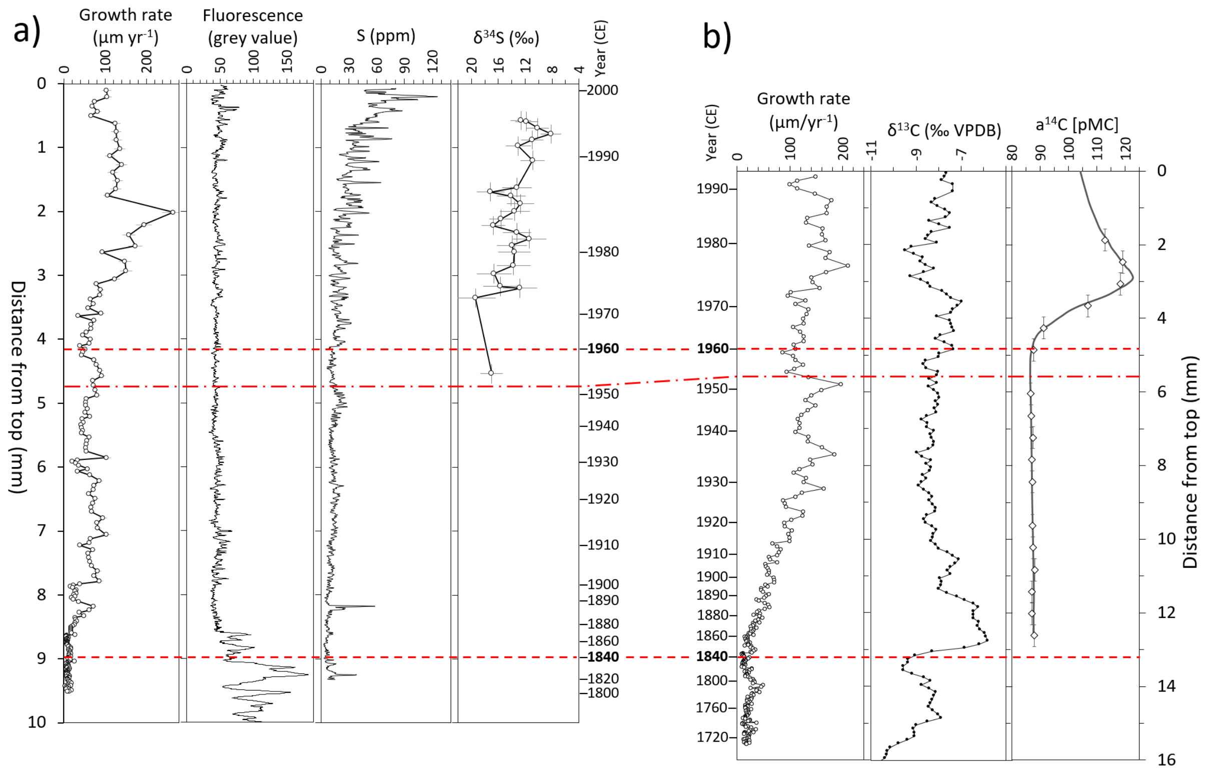

Figure 8. Summary of the Anthropogenic proxies in ER78 (a) and ER77 (b). In order to compare the two stalagmites, the series have been aligned using the years 1840 and 1960, reported in bold in the age column and highlighted by dashed horizontal red lines (note that in this way the ER77 series had to be "compressed" along the dft vertical axis in order to accommodate its faster growth rate with respect to ER78). Year 1840 CE corresponds to steady increase in the growth rate, the sudden decrease in fluorescence value in ER78 (change from microcrystalline impurity-rich to clear columnar laminae) and the sharp increase in $\delta^{13}C$ values in ER77 which marks the end of the Little Ice Age in the region. Year 1960 CE corresponds to the proposed position of the GSSP in ER77 based on the deflection point in the ^{14}C activity curve, whereas in ER78 corresponds to the increase in the annual growth rate and S concentration, and the following shift towards depleted $\delta^{34}S–SO_4$ that suggests an additional source of sulphur originating from industrial pollution. The horizontal dash-dot line on 1952 refers to the first global Pu fallout, the preferred boundary for the Anthropocene Series (Water et al., 2018).

Acknowledgements and Funding

This review paper has been facilitated by the Anthropocene Working Group (AWG) to ratify the stratigraphic Anthropocene. The AWG is co-ordinating the assessment of candidate GSSP sites in collaboration with the Haus der Kulturen der Welt (HKW, Berlin) in the framework of its long-term project Anthropocene Curriculum. The Anthropocene Curriculum is an international project for experimental forms of Anthropocene research and education developed by HKW and the Max Planck Institute for the History of Science (MPIWG, Berlin) since 2013.

The initial work on stalagmite ER76 was supported from the E.U. Environment Programme (Contract EV5V-CT94-0509). Long-term soil and cave monitoring were performed by Renza Miorandi with logistical assistance from Michele Zandonati (Science Museum of Trento) and supported by the University and Scientific Research Service of the Autonomous Province of Trento (Project AQUAPAST), the UK Natural Environment Research Council (NERC) and the Deutsche Forschungsgemeinschaft (DFG) Research Group 668 DAPHNE. The sulphur and sulphur isotope analyses were supported by the UK Natural Environment Research Council (NERC) (Grant NE/C511805/1). Additional sulphur dripwater analyses were performed by Dr. Flavio Corradini (Hydrochemistry Laboratory of Istituto Agrario di San Michele all'Adige, Trento). R. Hinton and J. Craven facilitated work at the NERC-supported ion microprobe facility at Edinburgh University and K. Linge (Kingston University) provided essential ICP-MS support (NERC grant NE/C511805/1). The synchrotron XRF analyses were performed at the European Synchrotron Radiation Facility (Experiment grant CH-1458) and facilitated by Jean Susini and Andrea Somogyi. The ^{14}C work was funded by the DFG research group 688 (DAPHNE) and the accelerator mass spectrometry (AMS) analyses were performed by Göran Skog at the AMS laboratory of Lund University. The high-resolution stable isotope analyses on ER77 were performed by Christoph Spötl at the University of Innsbruck (Austria) and the U/Th analyses on ER76 and ER77 were performed by Denis Scholz at the Heidelberg Academy of Sciences (Germany). The Cultural Heritage Service of the Autonomous Province of Trento granted access to the cave, while the stalagmite sampling has been authorized by the Geological Survey of the Autonomous Province of Trento. Gino Gasperini, the custodian of Grotta di Ernesto, is thanked for his kind co-operation.

Declaration of conflicting interests

The authors declared no potential conflicts of interest with respect to the research, authorship, and/or publication of this article.

Supplementary data

Supplemental material for this article is available online

References

Awsiuk R, Bartolomei G, Cattani L, et al. (1991) La Grotta d'Ernesto (Trento): frequentazione umana e paleoambientale. *Preistoria Alpina* 27: 7-160.

Bertò A, Buzzi A and Zardi D (2004) Back-tracking water vapour contributing to a precipitation event over Trentino: A case study. *Meteorologische Zeitschrift* 13(3): 189-200.

Baker A, Mariethoz G, Comas-Bru L, et al. (2021) The Properties of Annually Laminated Stalagmites-A Global Synthesis. Reviews of Geophysics 59(2): e2020RG000722.

Borsato A (1995) Ambiente di precipitazione e analisi microstratigrafiche di speleotemi in grotte delle Dolomiti di Brenta e Valsugana (Trento): interpretazioni genetiche e implicazioni paleoclimatiche. Università degli Studi di Milano, Milano.

Borsato A (1997) Dripwater monitoring at Grotta di Ernesto (NE-Italy): a contribution to the understanding of karst hydrology and the kinetics of carbonate dissolution. Proceeding 6th Conference on limestone hydrology and fissured media, La Chaux-de-Fonds, Switzerland Vol.2: 57-60.

Borsato A, Frisia S, Fairchild IJ, et al. (2007) Trace element disctribution in annual stalagmite laminae mapped by micrometer-resolution X-ray fluorescence: implication for incorporation of environmentally significant species. *Geochimica et Cosmochimica Acta* 71: 1494-1512.

Borsato A, Frisia S and Miorandi R (2015a) Carbon dioxide concentration in temperate climate caves and parent soils over an altitudinal gradient and its influence on speleothem growth and fabrics. *Earth Surface Processes and Landforms* 40(9): 1158-1170.

Borsato A, Frisia S, Wynn PM, et al. (2015b) Sulphate concentration in cave dripwater and speleothems: long-term trends and overview of its significance as proxy for environmental processes and climate changes. *Quaternary Science Reviews* 127 (2015): 48-60.

Borsato A, Johnston VE, Frisia S, et al. (2016) Temperature and altitudinal influence on karst dripwater chemistry: Implications for regional-scale palaeoclimate reconstructions from speleothems. *Geochimica et Cosmochimica Acta* 177: 275-297.

Dalmeri G (1985) La Grotta d'Ernesto: un insediamento preistorico di grande interesse per la conoscenza del Paleolitico finale nell'area trentino-veneta (Colle dei Meneghini-Val d'Antenne, Trentino sud-orientale). *Natura Alpina, Museo Tridentino di Scienze Naturali* 36(2-3): 31-40.

European Environmental Agency, 2014: http://www.eea.europa.eu/data-and-maps/indicators/eea-32-sulphur-dioxide-so2-emissions-1/assessment-3.

Fairchild IJ, Baker A, Borsato A, et al. (2001) Annual to sub-annual resolution of multiple trace-element trends in speleothems. *Journal of the Geological Society* 158: 831-841.

Fairchild IJ, Borsato A, Tooth AF, et al. (2000) Controls on trace element (Sr–Mg) compositions of carbonate cave waters: implications for speleothem climatic records. *Chemical Geology* 166: 255-269.

Fairchild IJ and Frisia S (2014) Definition of the Anthropocene: a view from the underworld. *Geological Society, London, Special Publications* 395(1): 239-254.

Fairchild IJ, Loader NJ, Wynn PM, et al. (2009) Sulfur fixation in wood mapped by synchrotron x-ray studies: Implications for environmental archives. *Environmental Science and Technology* 43(5): 1310-1315.

Faraji, M., Frisia, S., Hua, Q., Borsato, A. and Markowska, M. (2022) Accurate chronological construction for two young stalagmites from the tropical South Pacific. EarthArXiv https://doi.org/10.31223/X5MG97

Fohlmeister J, Kromer B and Mangini A (2011) The influence of soil organic matter age spectrum on the reconstruction of atmospheric ^{14}C levels via stalagmites. *Radiocarbon* 53(1): 99-115.

Fohlmeister J, Schröder-Ritzrau A, Spötl C, et al. (2010) The influences of hydrology on the radiogenic and stable carbon isotope composition of cave drip water, Grotta di Ernesto (Italy). *Radiocarbon* 52(4): 1529-1544.

Frisia S and Borsato A (2010) Karst. *Developments in Sedimentology*. pp.269-318.

Frisia S, Borsato A, Fairchild IJ, et al. (2000) Calcite fabrics, growth mechanisms, and environments of formation in speleothems from the Italian Alps and Southwestern Ireland. *Journal of Sedimentary Research* 70(5): 1183-1196.

Frisia S, Borsato A, Fairchild IJ, et al. (2005) Variations in atmospheric sulphate recorded in stalagmites by synchrotron micro-XRF and XANES analyses. *Earth and Planetary Science Letters* 235: 729 - 740.

Frisia S, Borsato A, Preto N, et al. (2003) Late Holocene annual growth in three Alpine stalagmites records the influence of solar activity and the North Atlantic Oscillation on winter climate. *Earth and Planetary Science Letters* 216(3): 411-424.

Frisia S, Borsato A and Susini J (2008) Synchrotron radiation applications to past volcanism archived in speleothems: An overview. *Journal of Volcanology and Geothermal Research* 177(1): 96-100.

Frisia S, Fairchild IJ, Fohlmeister J, et al. (2011) Carbon mass-balance modelling and carbon isotope exchange processes in dynamic caves. *Geochimica et Cosmochimica Acta* 75: 380-400.

Griffiths ML, Fohlmeister J, Drysdale RN, et al. (2012) Hydrological control of the dead carbon fraction in a Holocene tropical speleothem. *Quaternary Geochronology* 14:81-93.

Hartland A, Fairchild IJ, Lead JR, et al. (2012) From soil to cave: Transport of trace metals by natural organic matter in karst dripwaters. *Chemical Geology* 304–305(0): 68-82.

Hua Q, Cook D, Fohlmeister J, et al. (2017) Radiocarbon dating of a speleothem record of paleoclimate for Angkor, Cambodia. *Radiocarbon* 59(6): 1873-1890.

Huang Y, Fairchild IJ, Borsato A, et al. (2001) Seasonal variations in Sr, Mg and P in modern speleothems (Grotta di Ernesto, Italy). *Chemical Geology* 175: 429-448.

Johnston VE, Borsato A, Spötl C, et al. (2013) Stable isotopes in caves over altitudinal gradients: Fractionation behaviour and inferences for speleothem sensitivity to climate change. *Climate of the Past* 9(1): 99-118.

Johnston VE, Borsato A, Frisia S, et al. (2021) Last interglacial hydroclimate in the Italian Prealps reconstructed from speleothem multi-proxy records (Bigonda Cave, NE Italy). *Quaternary Science Reviews* 272: 107243.

Lageard JG, La Porta N, Thomas PA, et al. (2007) Dendroecology and dendrochemistry in Trentino: the Grotta di Ernesto project. *Studi Trentini Scienze Naturali, Acta Geologica* 82: 58-63.

Markowska M, Fohlmeister J, Treble PC, et al. (2019) Modelling the 14C bomb-pulse in young speleothems using a soil carbon continuum model. *Geochimica et Cosmochimica Acta* 261: 342-367.

Mayer B, (1998) Potential and limitations of using sulphur isotope abundance ratios as an indicator for natural and anthropogenic induced environmental change. Isotope techniques in the study of environmental change. Proceedings of IAEA Congress, Vienna Austria, 14-18th April 1997: 423-435.

McDermott F, Frisia S, Huang Y, et al. (1999) Holocene climate variability in Europe: Evidence from $\delta^{18}O$, textural and extension-rate variations in three speleothems. *Quaternary Science Reviews* 18(8-9): 1021-1038.

Miorandi R, Borsato A, Frisia S, et al. (2010) Epikarst hydrology and implications for stalagmite capture of climate changes at Grotta di Ernesto (NE Italy): results from long-term monitoring. *Hydrological processes* 24(21): 3101-3114.

Mylona S (1996) Sulphur dioxide emissions in Europe 1880–1991 and their effect on sulphur concentrations and depositions. *Tellus* 48B: 662-689.

Mylona S (1997) Corrigendum to Sulphur dioxide emissions in Europe 1880–1991. *Tellus* 49B: 447–448.

Noronha AL, Johnson KR, Southon JR, et al. (2015) Radiocarbon evidence for decomposition of aged organic matter in the vadose zone as the main source of speleothem carbon. *Quaternary Science Reviews* 127: 37-47.

Scholz D, Frisia S, Borsato A, et al. (2012) Holocene climate variability in north-eastern Italy: potential influence of the NAO and solar activity recorded by speleothem data. *Climate of the Past* 8: 1367-1383.

Smith CL, Baker A, Fairchild IJ, et al. (2006) Reconstructing hemispheric-scale climates from multiple stalagmite records. *International Journal of Climatology* 26(10): 1417-1424.

Smith CL, Fairchild IJ, Spötl C, et al. (2009) Chronology building using objective identification of annual signals in trace element profiles of stalagmites. *Quaternary Geochronology* 4(1): 11-21.

Vestreng V, Myhre G, Fagerli H, et al. (2007) Twenty-five years of continuous sulphur dioxide emission reduction in Europe. *Atmospheric Chemistry and Physics* 7(13): 3663-3681.

Waters CN, Turner SD, Zalasiewicz J and Head MJ (2022, submitted) Candidate sites and other reference sections for the Global boundary Stratotype Section and Point (GSSP) of the Anthropocene series. *The Anthropocene Review* (in this issue).

Waters CN, Zalasiewicz J, Summerhayes C, et al. (2018) Global Boundary Stratotype Section and Point (GSSP) for the Anthropocene Series: Where and how to look for potential candidates. *Earth-Science Reviews* 178: 379-429.

Wynn P, Loader N and Fairchild I (2014a) Interrogating trees for isotopic archives of atmospheric sulphur deposition and comparison to speleothem records. *Environmental Pollution* 187: 98-105.

Wynn PM, Borsato A, Baker A, et al. (2013) Biogeochemical cycling of sulphur in karst and transfer into speleothem archives at Grotta di Ernesto, Italy. *Biogeochemistry* 114(1-3): 255-267.

Wynn PM, Fairchild IJ, Borsato A, et al. (2018) Sulphate partitioning into calcite: Experimental verification of pH control and application to seasonality in speleothems. *Geochimica et Cosmochimica Acta* 226: 69-83.

Wynn PM, Fairchild IJ, Frisia S, et al. (2010) High-resolution sulphur isotope analysis of speleothem carbonate by secondary ionisation mass spectrometry. *Chemical Geology* 271(3-4): 101-107.

Wynn PM, Fairchild IJ, Spötl C, et al. (2014b) Synchrotron X-ray distinction of seasonal hydrological and temperature patterns in speleothem carbonate. Environmental Chemistry 11(1): 28-36.